

International Conference on Space Optics—ICSO 2022

Dubrovnik, Croatia

3–7 October 2022

Edited by Kyriaki Minoglou, Nikos Karafolas, and Bruno Cugny,



The Dual-blazed Diffraction Grating of the CHIME Hyperspectral Instrument: design, modelling & breadboarding.



The Dual-blazed Diffraction Grating of the CHIME Hyperspectral Instrument: design, modelling & breadboarding.

Benoit Borguet^{*a}, Vincent Moreau^a, Etienne Renotte^a, Gregory Lousberg^a,
Romain Vandoolaeghe^a, Roberto Di Paola^a, Luca Maresi^b

^aAMOS, Liege, Belgium ;

^bEuropean Space Agency, Noordwijk, The Netherlands

ABSTRACT

Copernicus, the European Union's programme for observing and monitoring the Earth, represents one of the most successful space programmes coordinated and managed by the European Commission in partnership with ESA, the Member States and Agencies. 2020 marked a major step of the Copernicus expansion programme with the selection of six missions to enter into B2CD implementation, namely CHIME, LSTM, CO2M, CRISTAL, ROSE-L, and CIMR.

The CHIME mission (Copernicus Hyperspectral Imaging Mission for the Environment) space segment was awarded to an industrial consortium led by Thales Alenia Space (FR), as Mission Prime, and OHB (DE), as Instrument Prime. Within the instrument team, the responsibility of the design and development of the spectrometer system (SPS) have been assigned to AMOS (BE). The SPS is the centrepiece of the CHIME instrument, ensuring the accurate spectral dispersion of the imaged ground swath over wide focal planes.

The SPS consists of three identical spectrometer units drawn from the compact de-magnifying freeform Offner optical solution developed at AMOS. Its throughput is guaranteed by a broadband convex diffraction grating, while the image quality and distortion control are enabled using freeform mirrors. This paper describes the mathematical modelling and prototyping activities, including manufacturing and testing of grating samples, carried by AMOS raising the maturity of the CHIME diffraction grating achieving Technology Readiness Level 6 (TRL6).

Keywords: Hyperspectral imaging, CHIME, dual-blazed grating, straylight, broadband efficiency, Single Point Diamond Turning, grating manufacturing

1. INTRODUCTION

Copernicus has been established to fulfil the growing need amongst European policymakers to access accurate and timely information services to better manage the environment, understand and mitigate the effects of climate change and ensure civil security. To ensure the operational provision of Earth-observation data, the Copernicus Space Component (CSC) includes a series of space missions called 'Sentinels', which are being developed by ESA specifically for Copernicus. The current phase of the programme encompasses the development of six missions (CHIME, LSTM, CO2M, CRISTAL, ROSE-L, and CIMR).

The CHIME mission [1] will provide routine hyperspectral observations through the Copernicus programme in support of EU and related policies for the management of natural resources. This unique visible-to-shortwave infrared spectroscopy-based capability will be dedicated to raw material- and sustainable agricultural management with a focus on soil properties, mineral resources and agricultural services, including food security and biodiversity.

To enable accurate quantitative estimates of specific vegetation bio/geo-physical/chemical variables, as well as top-soil variables and mineral compositions, CHIME encompasses as payload an imaging spectrometer [19]. This imaging spectrometer allows monitoring of land and coastal/inland water bodies with many contiguous spectral channels covering the 0.4-2.5 μm visible-shortwave infrared spectral range (VISWIR).

The spectrometer system (SPS) is the centerpiece of the CHIME instrument, ensuring the accurate spectral dispersion of the imaged ground swath over wide focal planes. The SPS consists of three identical spectrometer units (SU) drawn from the compact de-magnifying freeform Offner optical solution developed at AMOS [20]. The optical design of the CHIME

spectrograph unit is shown in Figure 1. It relies on a customized Offner-Chrisp layout, including a slit demagnification function of a factor 0.6. The 90 mm long input slit is spectrally reimaged in one of the 250 spectral bands thanks to the unique 47.68 grooves/mm spherical diffraction grating (GR) nominally operating in diffraction order $m = -1$. A thin fused silica order sorting filter plate (OSF) has been placed in the focal plane area, allowing for the efficient rejection of the light originating from spurious diffraction orders.

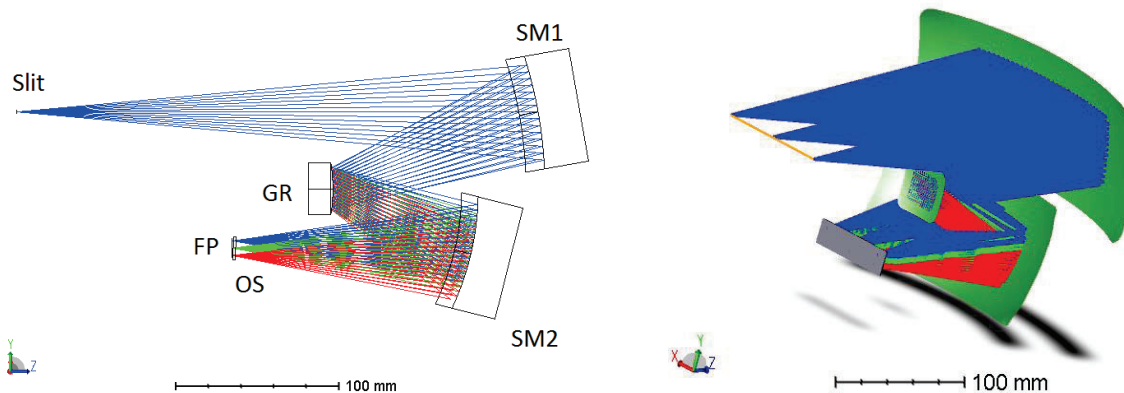


Figure 1. CHIME spectrograph optical design (left: Y-Z plane projection, right: 3D view). GR = Grating, OS = Order Sorting Filter, FP = Focal Plane. Ray colors correspond to wavelengths.

In order to guarantee the optical performances of each spectrograph subsystem with respect to the thermal variations encountered in operational conditions, a single material, all aluminum alloy concept is proposed. Therefore, the mechanical structure, the SM1 and SM2 mirrors, the diffraction grating, the aperture stop, the slit and its support are made of the RSA-443 alloy. This concept further enables the manufacture of highly accurate optical surfaces and references through diamond turning, facilitating the overall alignment procedure of individual spectrograph units.

The convex diffraction grating is the key enabler of the compact high performance SU. Specifically, its broadband diffraction efficiency ensures an adequate VISWIR throughput over a single focal plane. In order to ensure robust performances, the grating further requires properties of large low aberration aperture, high precision of groove density, high fidelity groove profile, limited polarization sensitivity, and low straylight contribution.

As a continuation of promising pre-development activities conducted in Phase A/B1 until late 2020, this paper reports on the successful completion of a technology programme dedicated to the development of a manufacturing process for the production of a CHIME-compliant broadband diffraction grating raising technical maturity of the diffractive optical element (DOE) up to TRL6. Major gratings specifications are reminded in Section 2. In Section 3 we detail the design of the groove profile and the numerical models used to assess the theoretical performances. The manufacturing process is summarized in Section 4 and the metrology approach in Section 5. The optical performances of machined technological samples are presented in Section 6. Results and future work are discussed in Sections 7 and 8.

2. BROADBAND GRATING SPECIFICATIONS

Table 2-1 : Diffraction grating specifications.

Specification	Value
Substrate	RSA 443 + NiP
Radius of Curvature	101 mm, convex
Useful optical area	32.5x28.5 (along x across groove)
Groove period	47.6876 gr/mm
Spectral range	0.4 -2.5 μm
Polarization sensitivity	< 3%
Spectral straylight	< 1E-4 at 633 nm

By design, the diffraction grating substrate shape has been chosen to be spherical. We gather the main specifications of the DOE in Table 2-1. Signal to noise ratio budgeting imposes an efficiency of the order over 40% at shorter visible wavelengths and above 20% at the reddest edge of the VISWIR range.

3. GRATING DESIGN AND PERFORMANCE MODELLING

Diffraction gratings are periodic repetitions of micro-structures of size Λ that can spatially modulate the amplitude or phase of the incident electromagnetic spectrum in a multitude of diffracted orders m . These orders are located at angular positions θ_m following the so-called grating equation:

$$\sin \theta_i + \sin \theta_m = m \lambda G,$$

where θ_i is the incidence angle, θ_m the diffraction angle for order m , λ the wavelength, and $G = 1/\Lambda$ the groove frequency. The inherent lack of selectivity of simple grating is translated by a usually poor throughput, far from the performance requirements set by high scientific throughput earth observation missions.

By applying a specific, linear phase function over each period, single blazed gratings maximize the DOE transmission in a selected diffracted order over a rather narrow spectral range. While perfectly blazed gratings do virtually exhibit a theoretical diffraction efficiency of 100% at the blaze wavelength, their limited spectral bandwidth (the shorter the blaze wavelength, the narrower the bandwidth) does not ensure significant throughput over the entire VISWIR spectral range.

Different solutions have been proposed and successfully applied in order to broaden reflective blazed gratings bandwidth, from dividing the optical aperture into selective blazed regions and/or using multiple diffracted orders [8][9][16][17] to finely engineering the groove profile [9][12][13][14]. For completeness we can also mention other approaches essentially considered on a theoretical basis for now, either varying groove density over the pupil [15] or considering sandwiched multi-layer blazed profile structures [1]. In the frame of the CHIME instrument, the spectral performance requirements demand the absence of additional pupil apodization or dephasing between selective blazed regions, therefore leading to the consideration of engineered groove profile. In the following, we detail the design of a SPDT compatible, diffraction efficiency compliant groove profile and further optimize its polarization sensitivity. We also implement a versatile grating spectral straylight model enabling the assessment of the straylight performances of manufactured gratings.

3.1 Achieving Broadband Diffraction Efficiency

Engineered groove profile represents the path investigated in our quest for a broadband diffraction grating, specifically, we consider a dual-blaze profile [9]. Such geometry is essentially described by three parameters that are the two blaze angles and their relative contribution to the full groove period. As noted in [13] while such a profile enables to achieve an adequate balancing of the overall energy across the complete VISWIR range the throughput does not typically exceeds 50% at any wavelength, still making the DOE a rather inefficient device.

Making this profile compatible with our manufacturing process, a concave dual-blaze profile is optimized against a target throughput specification using a custom python script. The script predicts diffraction efficiencies at selected spatial frequencies (diffracted orders m) and wavelengths using scalar theory ($\Lambda \gg \lambda$). The algorithm discretizes the groove profile and follows the formalism developed in [14] for evaluating the efficiency of the tested geometry, in parallel a Damped least Square algorithm is used in order to identify the best set of parameters fulfilling the specification (see top panel of Figure 2). In practice, the optimization is carried multiple times with varying seeds in order to prevent for local minima.

The groove profile discretization scheme employed makes the software versatile enabling adding groove roughness or profile edge smoothing by the convolution with appropriate kernel. Further the optimization loop can be carried simultaneously over several diffracted orders at a time. The diffraction efficiencies predicted by the scalar code have been checked against predictions from the computations carried through rigorous solving of the Maxwell equations within the PC Grate software [5], underlining the adequacy of the method for fast evaluation of the groove throughput. These high computational speed enables for groove profile parameter tolerancing via Monte Carlo simulation, emphasizing a $\sim 5\%$ sensitivity of the diffraction efficiency to the relative fractional contribution of each blaze angle section to the full groove period ($< 3\%$).

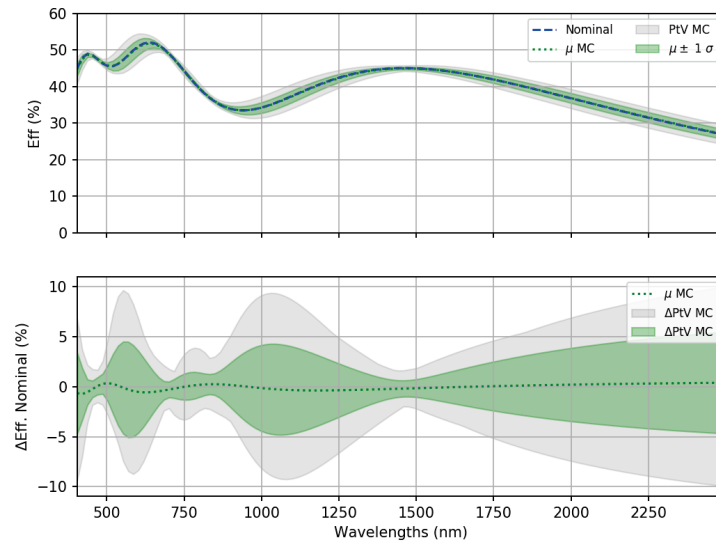


Figure 2 : Top: Prediction of the CHIME dual-blazed profile diffraction efficiency (dashed blue). The fast scalar computational method is used in the Monte Carlo tolerancing of the groove profile parameters. The most sensitive profile parameter identified is the relative contribution of each blaze section. Bottom: variations of the expected diffraction efficiency in nominal order $m=-1$ on the order of 5% considering 3% accuracy on fractional contribution parameter.

3.2 Polarization Sensitivity

While the sun provides a source of essentially unpolarized illumination, the reflected spectrum recorded by a hyperspectral instrument can exhibit significant linear polarization due to the scattering by elements in the scene under scrutiny or aerosols and molecules within the atmosphere. Due to its micro-textured surface, the diffraction grating is typically the largest contributor in the polarization sensitivity (DoP) of a hyperspectral sensor. Specifically, the polarization sensitivity of the grating originates from the different boundary conditions experienced by the propagating TE and TM modes across the textured surface. Modification of the traditional saw tooth blazed groove profile by either adding a flat top [3] or increasing the groove apical angle ([4][18]) reduces the sensitivity of the grating, at the slight expense of diffraction efficiency.

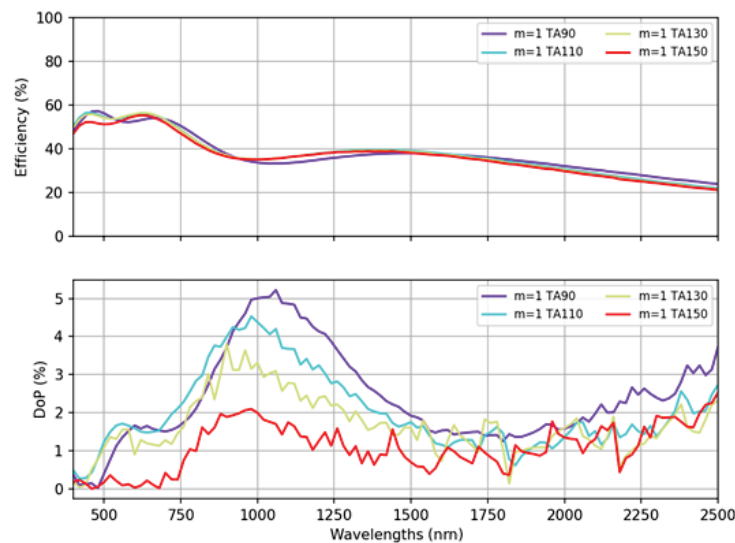


Figure 3 : Increasing the groove profile apical angle (TA) from 90° to 150° enables halving the polarization sensitivity of the grating, while only slightly degrading the diffraction efficiency. For the CHIME grating, an apical angle of 130° is considered.

In the CHIME context, we show in Figure 3 the evolution of the grating DoP considering the optimized dual blazed profile presented in Section 3.1 for which the apical angle (TA) is sequentially increased. The computations are carried within the PC Grate software. The simulation indicates that the modification of the optimized dual-blazed profile with an apical angle of 130° ensures a polarization sensitivity below 3% over most of the spectral range at a limited cost in terms of diffraction efficiency.

3.3 Spectral Straylight Model and Optimization

While most grating manufacturing papers focus on predicting and achieving high diffraction efficiencies, grating scatter, and especially inter-order straylight is another key property of DOEs. In well-designed spectrometers the grating is generally the main straylight contributor, resulting in the filling of spectral absorption features and the rounding of the emission peaks observed in the acquired spectrum. In addition to the natural blaze facet roughness, the random positioning errors in groove positioning generates a continuous inter-order background called grass, while periodical errors generate ghosts. In that respect grass-level can be particularly high for iteratively manufactured diffraction gratings.

A theoretical inter-order light model has been proposed by Sharpe & Irish (SI) [22]. Expanding on classical Fresnel-Kirchhoff diffraction theory, and considering traditional single blaze profile, they compute the normalized radiant flux from a monochromator. The model is parametrized enabling considering various sequential manufacturing errors: groove profile RMS roughness σ_r , RMS uncorrelated groove depth error σ_z , and RMS uncorrelated period error σ_p . Considering the CHIME coarse grating period, the most sensitive contributor to the inter-order straylight level is σ_z : doubling of the RMS value from 5 to 10 nm raises the grass level by an order of magnitude, while a σ_p of 100 nm RMS remains essentially an order of magnitude from the depth error contribution (see left panel of Figure 4).

While providing the direct physical insights on the origin of the scatter enabling setting target reference error levels to be reached during manufacturing, the complete analytical nature and built-in approximations of the SI model limits its usefulness in the rigorous modeling of the inter-order straylight level generated by engineered groove profile diffraction gratings and the consideration of specific manufacturing error sources. Therefore, we developed a custom numerical model of the grating straylight distribution in the dispersion plane. This model builds upon scalar Fourier optics concepts, specifically the Fraunhofer approximation, enabling the estimation of the spatial frequency representation of the far field $E(f_x)$ at spatial frequencies $f_x = \cos(\theta) / \lambda$ as the Fourier transform of the complex transmittance function $t(x)$:

$$E(f_x) = \int t(x) e^{-i2\pi f_x x} dx.$$

The far field intensity is then computed as the amplitude of the scalar field: $I(f_x) = |E(f_x)|^2$. The complex transmittance function of an unidimensional grating can be represented by:

$$t(x) = g(x) * \text{III}\left(\frac{x}{\Lambda}\right) \text{rect}\left(\frac{x}{G}\right),$$

where $g(x)$ describes the single groove phase function, $*$ is the convolution product, $\text{III}(x/\Lambda)$ is the Dirac comb of period $1/\Lambda$, and $G = N\Lambda$ is the size of a grating with N grooves.

Due to the properties of the Fourier transform, the expression of $E(f_x)$ can be expressed as the coherent summation of the contribution of each single groove far field response. This response is evaluated on a discretized grid (see Section 3.1). Realistic manufacturing errors are added to each groove separately, sampling representative power spectral densities, through the multiplication of appropriate phase factors. We benchmark our numerical model against the SI model considering single blaze groove profile and representative manufacturing RMS errors σ_z, σ_p and find an excellent agreement between both models when considering the bandwidth of the setup (see right panel of Figure 4). For a CHIME compliant grating, the numerical model translates the spectral straylight requirement asking the uncorrelated error on the groove depth to be below 5 nm RMS.

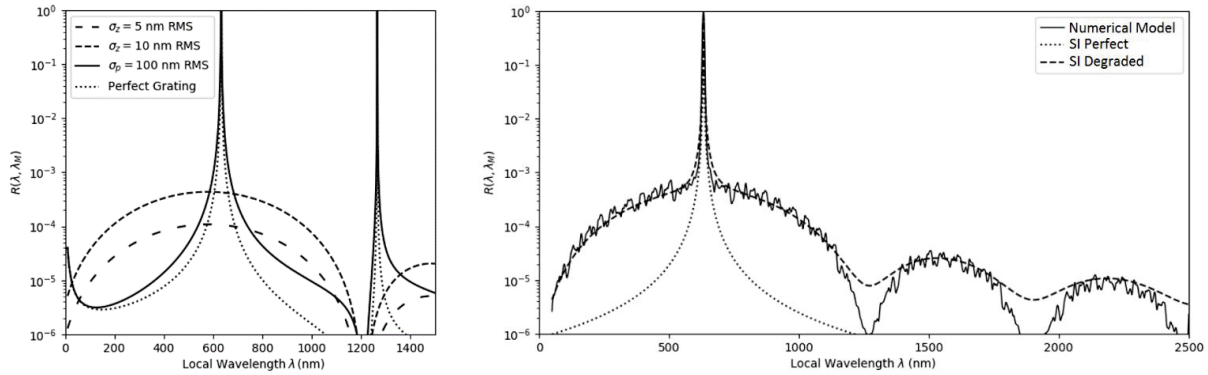


Figure 4 : Left: Sharpe & Irish (SI) model of the inter-order straylight level observed in a monochromator set at $\lambda_M = 633 \text{ nm}$ where a coarse, 50 gr/mm grating is affected by various manufacturing errors. Reference background level for a perfect grating is set by the dotted line. We note the large sensitivity of the background level to the depth error. Right: comparison of the predicted background level at 633 nm of our semi-analytical software and the prediction from SI model for a grating blazed at the same wavelength in order $m=-1$, explaining why only this order is predicted.

A semi-analytical diffraction grating Bidirectional Reflectance Distribution Function (BRDF) model for single blazed groove profile has recently been proposed in [23], providing similar formulation when considering the traditional sawtooth profile. Our model can be considered as a generalization of this algorithm to arbitrary groove profiles. Interestingly [23] underline in their equation (7) the elegant connection between the far field intensity and the BRDF as:

$$BRDF(\theta, \varphi) = \frac{1}{\lambda^2} I$$

providing a unique bridge between physical optics and radiometry. Therefore, considering appropriate scaling, our numerical model output can be used to realistically model the spectral scatter function from the dual-blazed diffraction grating. This model can then be input within straylight modelling code such as FRED enabling accurate simulation of instrumental straylight performances.

4. DUAL BLAZED GRATING MANUFACTURING

The fabrication of coarse dual-blazed groove profile gratings has been developed and demonstrated for about 20 years via e-beam lithography techniques [8][12] and more recently by a microfabrication-based approach using grayscale photolithography technique [24]. Both methods have their advantages and drawback but enable reliably producing low straylight gratings with inter-order background levels 4 to 5 orders magnitude lower than the main diffraction peak [13].

Our manufacturing approach considers the use of Single Point Diamond Turning (SPDT) on Ultra-Precision Machining lathe (UPM) heritage available at AMOS for blazed freeform gratings [17][20] and bring it to the physical limits for the production of the CHIME dual blazed gratings. While also adapted to the grooving of coarse gratings (G up to ~ 100 gr/mm), when compared to the aforementioned techniques, SPDT has the extra advantage of the direct manufacturing on appropriate Aluminum-based substrate material suited for thermally-insensitive instrument design, altogether with the inclusion of ultra-accurate reference surfaces, easing the AIV process. Further this technique produces high fidelity groove profile over the complete grating aperture by the replication of the cutting sharp tool profile and can also accommodate highly curved and freeform substrate surface shape ([17][20][21]). In the following, we describe our manufacturing setup, then investigate the hard-physical limit of the UPM-based groove shaping technique with respects to random groove depth placement error by manufacturing single-blazed flat samples. Finally, we describe the manufacturing of a representative dual blazed grating on a convex surface, demonstrating the currently achieved state of the art performances.

4.1 Manufacturing setup

The diffraction gratings are manufactured through SPDT on an ultra-precision CNC Moore Nanotech 350 FG lathe (see Figure 5). The machining center sits in a temperature-controlled room of the optical workshop and disposes of five-axis ultraprecision servo-control. The freedom enabled by the three linear (X, Y, and Z) and two rotational (B, and C) axes allows the accurate manufacturing complex surface figures making it adapted to the fabrication of freeform gratings and complex opto-mechanical elements. A thorough characterization of the axis positioning error and kinematical behavior of

the lathe has been carried in a preliminary research phase enabling identifying best cutting configuration for the grating samples.

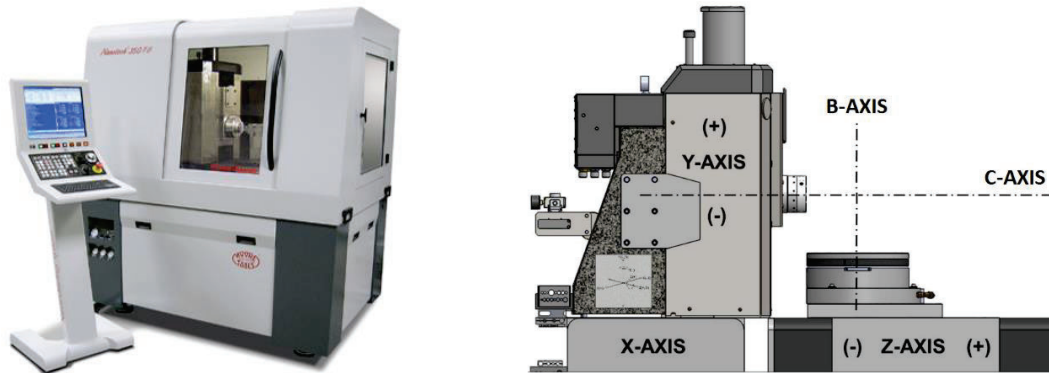


Figure 5 : Left: Moore Nanotech 350 FG 5-axis ultra-precision turning lathe available at AMOS. Right: Sectional YZ view of the axis configuration. The lathe is equipped with 3 linear axes: X, Y, Z and two rotational axes: B and C. Source: www.nanotechsys.com.

Each grating grooves are cut sequentially in a monolithic way (including counter blaze angle) from the workpiece within a single pass requiring a custom shaped dead-sharp dual-slope natural monocrystalline diamond tool. The process for forming the grooves is shaping (material removal at the contact point) as it is known to produce high fidelity groove profile than traditional ruling (deformation of the substrate surface by applying a normal force). The grooves are cut in Electroless Nickel plated (NiP) Aluminum alloy workpieces. NiP is recognized as the material providing best grooving results due to its higher hardness, limiting risks of Poisson burrs formation on the edge of the grooves caused by plastic flow of the material during the shaping process [6][10][11].

4.2 Flat Samples Performances

Preliminary to the machining of representative CHIME grating samples on convex substrates, a set of flat single-blazed samples have been manufactured in the XYZ configuration. This step is carried after the characterization of the individual lathe axes errors and is useful in order to consider both static and kinematical errors occurring during a cut. The metrology of the samples enables us gauging the raw performances achieved in a cutting configuration using a limited number of axes therefore the ultimate performances that can be achieved with the UPM lathe and whether those are compatible with the production of low-straylight samples. Further this step enables the fine tuning of the cutting parameters and strategy.

Flat 30x30 mm² workpieces with identical material and plating to the CHIME grating samples are fixed on the XY translation stage of the lathe while a sharp single blazed, 130° included angle monocrystalline diamond is mounted on the Z axis. Grooves are machined by the upward motion of the Y axis, the indexation of the X axis enabling the grating periodicity, while Z axis ensures the sample surface form error and manages the absence of tool/workpiece collision during the downward motion.

The performances of the flat samples are characterized both in terms of Surface Form Error (SFE) and uncorrelated depth error. The former is measured through null interferometry against a flat reference wavefront, while the latter is assessed from the simultaneous linear fit (dubbed terrace fit, see left panel of Figure 6) of multiple groove cuts obtained through White Light Interferometric (WLI) device (Zygo Nomad). SFE below 20 nm RMS are achieved over the complete aperture and without any obvious chatter mark. Along groove roughness in the range 1.5-2 nm RMS is observed. Uncorrelated depth errors below 2.5 nm RMS is also reported consistently over sets of 330x330 μm² patches of Nomad observations scattered across the grating surface. Note that in addition to the depth error, the terrace fit also enables testing for the manufactured groove profile, and particularly provides a direct measure of the cutting tool angle, enabling for compensation if needed. Flat samples performances indicate SPDT to be in line with the major CHIME grating requirements.

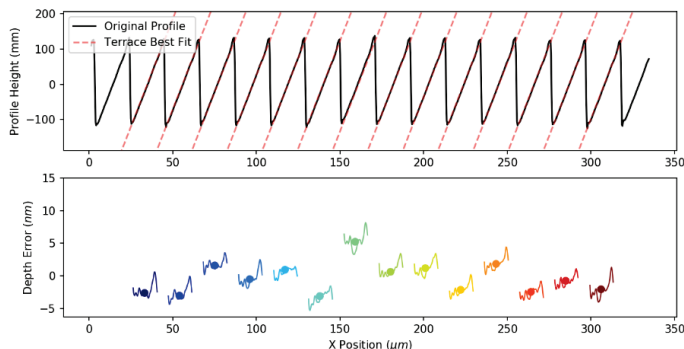
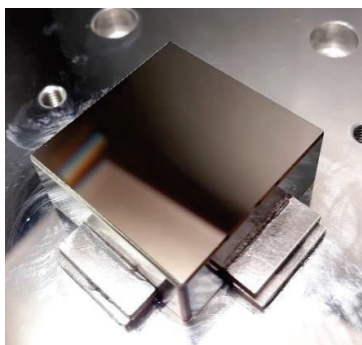


Figure 6 : Left: Flat 0.7° blazed sample machined in the XYZF configuration. The Moore 350 FG enables the machining of high-fidelity micro-structures within the NiP. Right: Top: Terrace fit to 1D cross groove cuts of localized WLI data underlines the achievement of extreme positioning accuracy. Bottom: Residuals exhibit PtV depth error within 10 nm, and an RMS value < 2.5 nm compatible with the low inter-order straylight requirements.

4.3 Convex sample manufacturing setup

The thorough UPM lathe characterization campaign targeting the axis positioning error and kinematics behavior lead to the identification of the best cutting configuration for highest convex grating performances in terms of depth error, and surface form error. The identified configuration is the XCFZB, where the workpiece is mounted on the kinematic chain XC, while the sharp diamond tool is mounted on the kinematic chain ZB. Note that we also tested more traditional ruling/shaping configurations although a major advantage of the XCFZB is the smooth continuous rotation of the workpiece around the C axis and the identical cutting conditions along the groove length ensured by the constant rake angle along each groove guaranteeing the best grating performances..

The manufacturing fixtures, alignment procedure and shaping process (cut depth, feed rate, ...) employed at AMOS are proprietary but essentially conforms to the steps outlined elsewhere in the literature (e.g. [12], [13] [17], [27]). Specifically, following the curved profile of a convex diffraction grating requires indexing the tool X, Z positions from groove to groove, but also the B-axis angle for each groove maintaining the dual-blazed profile constant with respect to the local normal of the substrate surface in the cross-groove direction. This guarantees best efficiency over the integrated useful optical area. Note that the synchronized motion of the X and C axes during a groove cut enables the manufacturing of freeform diffraction gratings ([23], [27])

The NiP-plated spherical convex samples have a RoC of 101 mm, and a 60×36 mm² square mechanical aperture. The useful aperture is 32.5×28.5 mm². A custom high precision dual-slope diamond tool is used for the shaping process. The baseline machining configuration considers the cutting of the complete mechanical area and is achieved in a few hours limiting the impact of thermal related considerations.

5. GRATING METROLOGY

The metrology of the manufactured grating samples follows two distinct metrology streams at AMOS. Stream 1 characterizes the machined sample at micro-scale. The use of multiple narrow field of view (330×330 μm²) WLI observations provides a localized characterization of the achieved microstructures fidelity and periodicity. Specialized Python-based reduction pipeline highly automates the data analysis process, providing direct and robust access to the along groove roughness, period and depth errors, or manufactured profile geometry. This micro-scale information is used as input within the diffraction efficiency and spectral straylight models for predicting achieved grating performances on a macro-scale.

Stream 2 evaluates the grating performances over a so-called macro-scale: considering the complete useful optical area of the sample. Surface Form Error is measured with a dynamic Fizeau interferometer (Zygo Dynafiz [25]). A dedicated Offner-based Grating Test Setup (GTS) developed at AMOS (see Figure 7) enables the direct measurement of the convex grating performances in terms among others of diffraction efficiency and inter-order straylight level. The useful grating area is illuminated with a series of monochromatic source considering representative optical interface conditions in terms of angle of incidence (AOI) and F#. An image of a thin slit or pinhole object is formed at the focal plane of the GTS enabling complete 2-dimensional assessment of the light distribution in the vicinity of selected diffraction orders. The

application of high dynamical range imaging (e.g. [26] and references therein) provide a unique, high sensitivity (over 7 orders of magnitude within our current setup) access to the inter-order background, and specifically to any large spatial scale fabrication error affecting the processed workpiece.

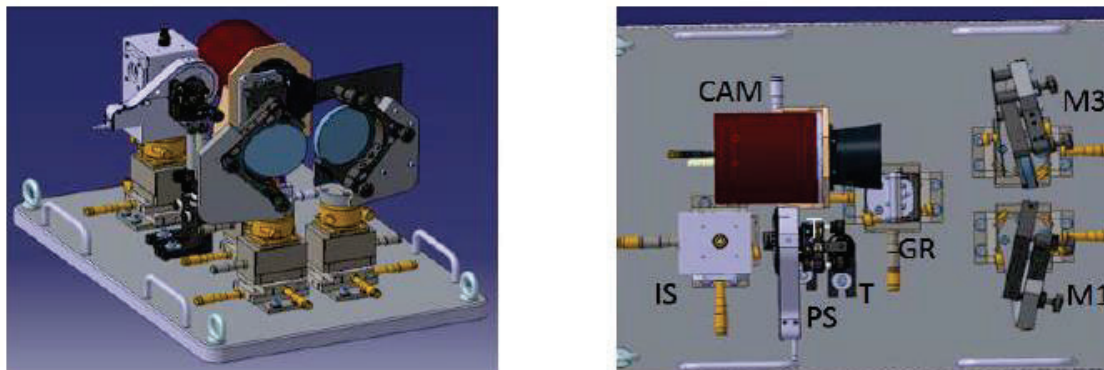


Figure 7 : 3D views of the Grating Test Setup (GTS) developed at AMOS for testing the performances of the manufactured convex gratings. The GTS consists in an Offner relay (M1, M2, GR), where secondary optical element (GR) can be switched between the grating under test or a reference mirror. Monochromatic laser/filter based light source feeds an integrating sphere (IS) illuminating a test pattern (T). The latter is imaged on a camera (CAM). The use of separate InGaAs and CMOS focal planes enables covering the 400-1650 nm spectral range. The above figures do not show the baffling.

6. MANUFACTURED GRATING PERFORMANCES

We report the state-of-the-art performances achieved for a CHIME compliant grating manufactured in the frame of this pre-development project. Exquisite surface finish can be reproduced with high repeatability over various cuts underlying the robustness of the shaping process. Measured performances at macro-scale are directly compared to numerical models obtained from micro-scale characterization.



Figure 8: Pictures of an actual dual-blazed UPM-shaped grating. The grooves are parallel to the workpiece long edge, (spatial direction), while the spectral dispersion direction is orthogonal to it. Order identification is proposed on the right panel.

6.1 Micro-scale characterization

WLI metrology has been performed over 10 sampling regions distributed over the useful optical machined surface. We report below the average performances consistently achieved over the grating area.

Manufactured groove profile:

The groove profile for the vertex position of the workpiece is compared with the theoretical profile in Figure 9. The measured profile is in excellent conformity with respect to the nominal design. Matching the specified diffraction efficiency requires a maximal error $\pm 0.5 \mu\text{m}$ of the dual-slope inflexion point and the reported profile is compliant with this tolerance. The tool positioning angle, defining the lowest of both blaze slopes, is measured from the profile with a mean value of $0.789^\circ \pm 0.002^\circ$, compliant with the requirement of a CHIME compliant profile.

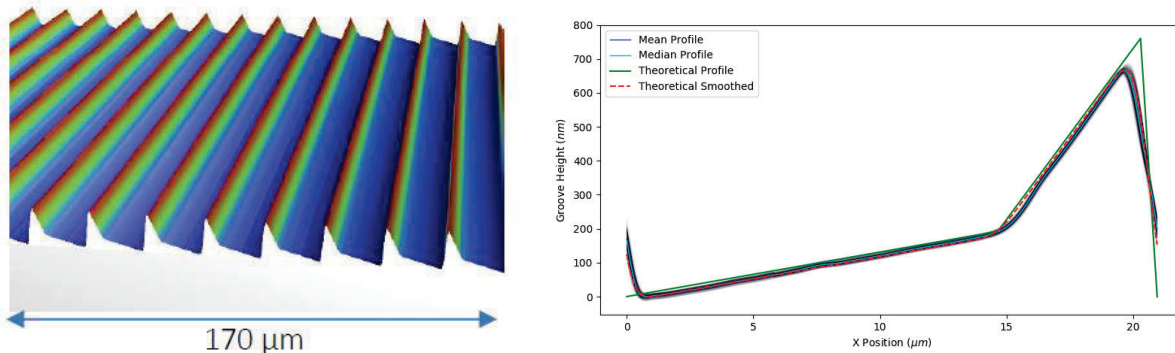


Figure 9: Measured groove profile on the dual-blazed machined sample. Left: 3D view of the height map acquired by WLI at the vertex of the optical surface. For better perception, the Z-Axis (height) is scaled by a factor of x15 with respect to the X-axis. Right: Average and median groove profile compared with theoretical dual-blazed profile. The dashed -red curve is the expected measurement considering the WLI spatial resolution (0.33 μm/pixel).

ALG roughness:

The along groove roughness is the major contributor for the spatial straylight generated by the diffraction grating. This roughness is influenced by cutting parameters (speed, depth of cut, tool sharpness), substrate material properties (micro-hardness, defects...), and by the micro-vibrations (lathe, acoustic noise, support tools eigen frequency, micro-seismic...). An ALG roughness < 3.5 nm RMS is required for a specification-compliant grating, which matches the performance measured on the samples where average ALG roughness in the range 3-3.5 nm RMS are observed over the grating area. Note that the low spatial frequency errors (< 5 mm⁻¹) are the largest contribution to ALG roughness. Residual higher frequencies are contributing for about 1.5 nm RMS.

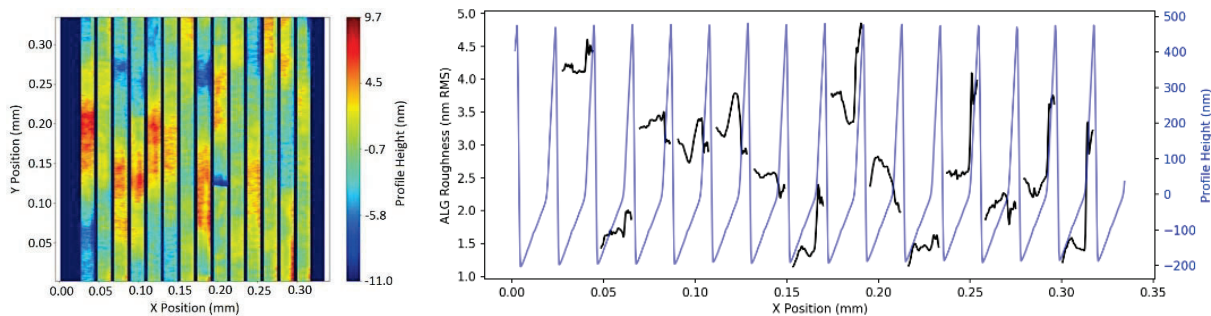


Figure 10 : Left: Intra-groove roughness map, the along groove direction if following the ordinate. Best groove profile model has been extracted revealing the groove roughness. The color scale covers 20 nm PtV. Right: The along groove roughness is computed and plot for each column of the leftmost figure. Average groove profile is represented in light blue. The average ALG roughness over all grooves is < 3 nm RMS for this specific sample, with high spatial frequency contribution typically less than 1.5 nm RMS.

Groove depth error:

Our inter-order straylight simulations highlight the uncorrelated depth error as a major contributor to the out-of-band (OoB) signal (see Section 3.3). Achieving the OoB signal requirement necessitates a groove-to-groove depth error less than 5 nm RMS is reached. We verify this from WLI metrology data from which we successively extract and fit sets of across groove profiles. Departures from the strictly periodic best fit model translates the misplacement of the groove depth from ideal location. RMS deviation is computed for the set of grooves, the operation is repeated for all lines within the WLI image, and statistics is reported for the complete set of images. An extreme regularity is noticed over the workpiece, with maximal random depth errors reaching 4 nm RMS for the worst sampled point, and a mean value of 3.2 nm RMS over all sampled points. Based on the numerical model, these results anticipate a low level of inter-order straylight, further confirmed through direct imaging in Section 6.2.

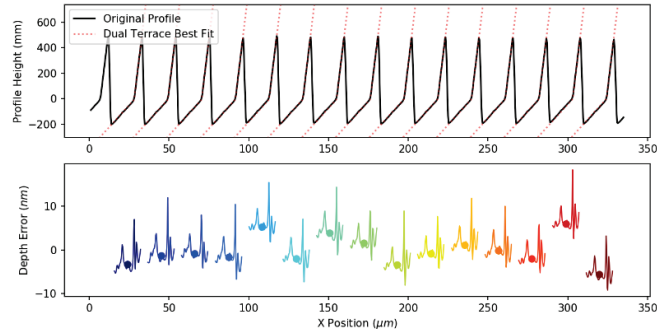


Figure 11 : Illustration of the groove random depth error analysis using the Python-based terrace fit script adapted for a dual-blazed groove profile. Top: Successive across groove profile stripes are fit with a strictly periodic dual blazed function. The median residual height level of each groove is calculated resulting in a groove-to-groove standard deviation (groove depth error) of 3.2 nm RMS for the illustrated sample.

6.2 Macro-scale characterization

In the following we compile macro-scale characterization results providing comprehensive results over the complete useful optical area of the diffraction grating. Diffraction efficiency and inter-order straylight level are measured directly and the results are correlated with measured micro-scale parameters.

SFE

The SFE of the gratings have been measured in diffracted order $m=0$, revealing the accuracy of the surface sphericity. The convex workpiece is positioned concentric to a fast $F\#1.5$ reference sphere so that an appropriate spherical wavefront impinges the grating surface in that order. The rough results present a slight deviation from the 40 nm RMS requirement (see left panel of Figure 12). However, we note the main contributor to the error is residual 90° astigmatism (Zernike Fringe term $Z5$) that results from a small divergence between the programmed tool trajectory and the distance between the workpiece vertex and the spindle axis. Such discrepancy can be further reduced through a finer alignment procedure of these geometrical parameters. Ultimately, after removal of the $Z5$ term from the SFE, the error drops to 21 nm RMS demonstrating that the 40 nm RMS requirement is achievable with a more precise alignment.

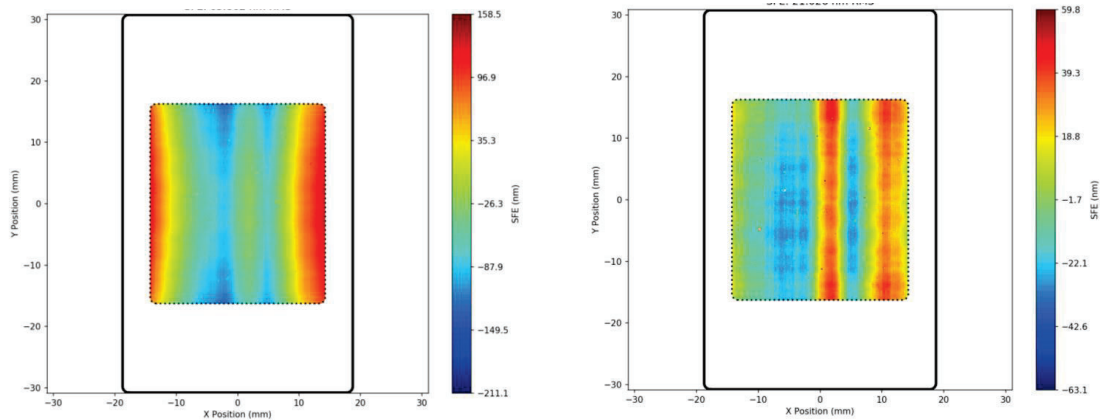


Figure 12 : Left : SFE measured at order 0 over the useful aperture: 66 nm RMS (Piston-Tip-Tilt-Focus from setup misalignment have been subtracted out). Right: The residual SFE reaches 21 nm RMS after correction of 90° astigmatism. Note: SFE is only presented over the 28.5×32.5 mm² useful optical area (dashed line), the mechanical aperture of the workpiece is defined by the solid black line.

Diffraction efficiency

Measurement of the grating diffraction efficiency is carried with the GTS over the 400-1650 nm spectral range, using a 100 μ m pinhole as target. Relative diffraction efficiencies are calculated based on the ratio of aperture photometry DN values within the diffracted spots and the reference level set by a highly polished ($R_q < 1$ nm RMS) NiP plated spherical mirror. Measured diffraction efficiencies are reported in Figure 13 and compared with efficiency prediction computed

based on the as built groove profile metrology. We report an excellent agreement between the simulations and measurements for 12 discrete wavelengths distributed over the tested spectral range. This correlation is confirmed not only for nominal diffracted order $m=-1$, but also over the surrounding $m=0$ and $m=-2$ orders also acquired by the GTS. Finally, the measured efficiencies show an extra margin of about 5% in absolute value with respect to the requirements.

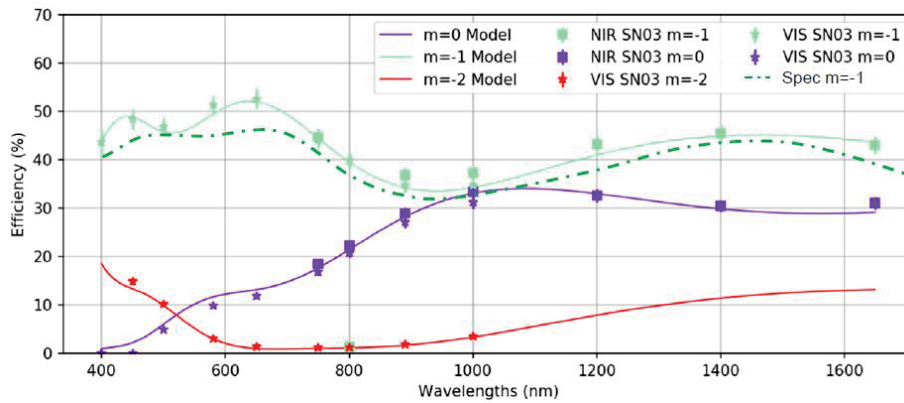


Figure 13 : Diffraction efficiency curves of the dual blazed grating within diffracted order $m=0$, -1 and -2 computed from the micro-scale groove metrology (solid lines). Measurements of the efficiency with the GTS at specific spectral wavelengths are overplot (stars = CMOS camera, boxes = InGaAs camera). We observe a good agreement between predicted efficiencies and measured ones.

Inter-order background

The inter-order straylight and parasitic ghost features are measured with the GTS with laser sources at 406 and 640 nm. A 30 μm wide slit is used as the target and set orthogonal to the dispersion plane. HDR bracketing is employed in order to extend the sensitivity of the test bench to about 7 orders of magnitude. In Figure 14 we report the measured inter-order level normalized to peak ($m=-1$) intensity for both test wavelengths and compare the measurement with straylight level predicted with our numerical model (see Section 3.3) considering a 5 nm RMS random depth error. At 640 nm the detected straylight level is significantly below $1e-4$ between adjacent orders. This level is almost reached at 406 nm indicating the satisfactory behavior of the grating scattering function at the most challenging wavelengths. In addition, no ghost feature can be identified between the main orders indicating the absence of significant periodic error on the grating.

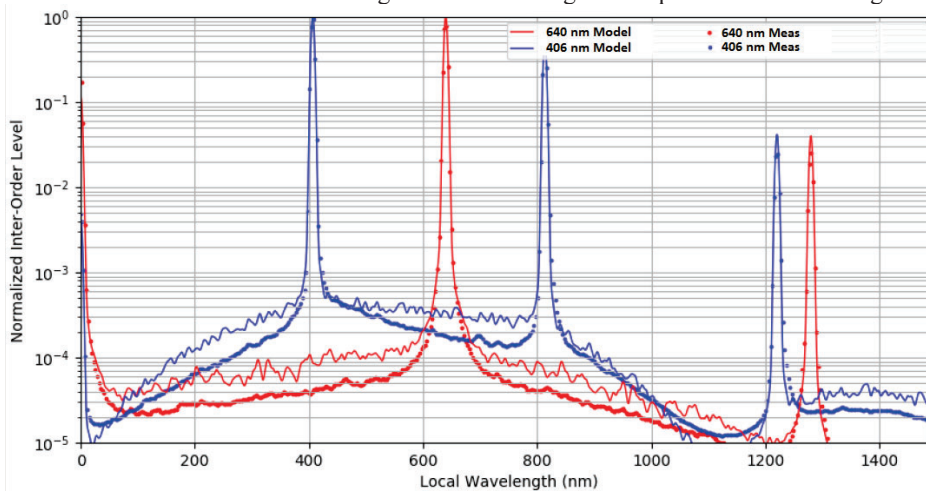


Figure 14 : Measured grating inter-order straylight at 406 nm (blue) and 640 nm (red) with the GTS (dots). The measured straylight levels are compared with the specified maximum levels simulated for a 5 nm RMS grooves depth error at those wavelengths (solid lines). All data are normalized with respect to the intensity of the nominal diffracted order, $m=0$ order is located at 0 nm.

7. CONCLUSIONS

In this paper we presented the design, manufacturing and characterization of a dual blazed diffraction grating. The specific groove profile has been optimized providing broadband VISWIR efficiency making the grating compatible with the compact, high performance spectrometer design of the CHIME mission. The optimization of the profile also considers the reduction of the grating polarization sensitivity to less than 3% by increasing the counter-blaze angle. As a result, this diffraction grating makes the spectrometer unbeatable in terms of performance and makes the design much simpler than any other configuration.

Simple scalar diffraction theory-based tools have been presented and used in the fast optimization of compliant groove profile geometry with respect to target diffraction efficiency within a specific diffraction order. Extension of this numerical model enables the estimation of the inter-order straylight level observed between the main diffraction orders in sequentially manufactured gratings. Specifically, we show that the main contributor to the grass level in a coarse, 50 gr/mm CHIME-like, grating is the uncorrelated depth error. As shown in [23] the model can be transposed in terms of BRDF enabling a more accurate simulation of the grating-based spectrometer straylight.

We demonstrate the adequateness of SPDT on ultra-accurate lathe to produce dual-blazed gratings on convex substrates. Compared with other methods, direct SPDT shaping process gives the exclusive possibility to accurately adjust the tool angle from groove to groove in order to follow the spherical shape of the substrate, also enabling freeform geometry. The ruling approach further has the advantage of being compatible with the structural material (Nickel plated AISi alloy) selected for the complete CHIME spectrometer, so that the assembling, mechanical and thermal stability of the unit are highly strengthened.

The complete characterization of SPDT shaped gratings underlines the consistency of the groove profile geometry, ensuring the broadband efficiency is reached. Inter-order straylight measurement at 640 nm exhibits almost 5 orders of magnitude relative to the main peak, on par with other production methods. Correlation with the numerical model illustrate state of the art results in terms of the control of the groove depth positioning error to within less than 5 nm RMS.

At the end of this activity, we demonstrate that SPDT shaping of dual-blazed gratings has reached a Technology Readiness 6, in the sense that the technology has been demonstrated on representative samples. Further enhancement of our workpiece alignment procedure will ensure the reduction of the 90° astigmatism affecting the SFE.

8. FUTURE WORK

With this work we demonstrated the maturity of our technology to produce metal dual blazed diffraction gratings that meet the technical specifications that fulfill the CHIME mission objectives, see Section 2. We de-risked and established a robust and repeatable manufacturing process ready to satisfy the demanding production of the flight components. On the process itself, a little improvement is needed to eliminate the residual astigmatism, see Fig. 12. This is believed to be achieved by investing in the alignment effort. Besides, significant upgrades will be brought to the verification set-up, including the extension of the spectral range and the addition of control features and automated functions that will allow serial testing of flight components in the most reliable fashion.

*benoit.borguet@amos.be; phone +32 4 361 40 40; amos.be

ACKNOWLEDGEMENTS

The CHIME programme is developed under the auspices of the European Space Agency (ESA) by an industrial consortium led by Thales Alenia Space (France), as Mission Prime, and OHB System AG (Germany), as Instrument Prime. The CHIME spectrometer systems are developed by AMOS s.a. (Belgium) for OHB under ESA sub-contract No. CHIM-CO-OHB-IN-0004. AMOS is grateful to the MFG group of the *Technische Universität Berlin* (PTZ 7) for their most valuable contribution to this work. Their knowledge of micro-technologies and their advices were invaluable to us.

REFERENCES

- [1] Tailhades, S., "The Copernicus Expansion and OHB Contribution. Overview and Current Status." 72nd International Astronautical Congress (IAC), Dubai, United Arab Emirates (2021)
- [2] Sandfuchs, O., Kraus, M., and Brunner, R., "Structured metal double blazed dispersion grating for broadband spectral efficiency achromatization" *Journal of the Optical Society of America A*, Vol. 37, No. 8 (2020)
- [3] Diehl, T., Triebel, P., and Moeller, T., "Optical gratings and grisms: developments on straylight and polarization sensitivity improved microstructures" *Proc. SPIE* Vol. 9611 (2015)
- [4] Zhu, J., Chen, X., Zhao, Z., and Shen, W., "Long slit polarization-insensitive imaging spectrometer for wide-swath hyperspectral remote sensing from a geostationary orbit" *Optics Express*, Vol. 29, No. 17 (2021)
- [5] PCGrate-SC Version 6.5, IIG Inc, (2014)
- [6] Li, H., Peng, X., Guan, C., and Hu, H., "Ultra-Precision Cutting and Characterization of Reflective Convex Spherical Blazed Grating Elements", *Micromachines* 13, 1115 (2022)
- [7] Gebhardt, A., Steinkopf, R., Scheiding, S., Risse, S., Damm, C., Zeh, T., and Kaiser, S., "MERTIS – Optics manufacturing and Verification" *Proc. SPIE* Vol. 7808 (2010)
- [8] Wilson, D.W., Maker, P.D. Muller, R.E., Mouroulis, P., and Backlund, J., "Recent advances in blazed grating fabrication by electron-beam lithography", *SPIE Proc.* 5173, 115-126 (2003)
- [9] Mouroulis, P., Wilson, D.W., Maker, P.D., and Muller, R.E., "Convex grating types for concentric imaging spectrometers" *Applied Optics*, Vol. 37, No. 31 (1998)
- [10] Jagodzinski, M., Kühne, S., Weber, J., Rolon, D., Malcher, D., and Oberschmidt, D., "Suitability of electroless nickel for diffractive optics manufacturing", *Euspen's 20th international conference and exhibition* (2020)
- [11] Xu, D., Owen, J.D., Papa, J.C., Reimers, J., Suleski, T.J., Troutman, J.R., Davies, M.A., Thompson, K.P., and Rolland, J., "Design, fabrication, and testing of convex reflective diffraction gratings", *Optics Express*, Vol. 25, No. 13 (2017)
- [12] Lockwood, R.B., Cooley, T.W., Nadile, R.M., Gardner, J.A., Armstrong, P.S., Payton, A.M., Davis, T.M., Straight, S.D., Chrien, T.G., Gussin, E.L., and Makowski, D., "Advanced Responsive Tactically-Effective Military Imaging Spectrometer (ARTEMIS) design", 2006 IEEE International Symposium on Geoscience and Remote Sensing (2006)
- [13] Chrisp, M.P., Lockwood, R.B., Smith, M.A., Balonek, G., Holtsberg, C., Thome, K.J., Murray, K.E., and Ghuman, P., "Development of a compact imaging spectrometer form for the solar reflective spectral region", *Applied Optics*, Vol. 59, No. 32 (2020)
- [14] Backlund, J.P., Wilson, D.W., and Muller, R.E., "Structured-groove phase gratings for control and optimization of the spectral efficiency" *Frontiers in Optics 2004*, paper DMB6
- [15] Li, B., Wang, B., Wang, T., Zhang, H., and Wang, W., "Visible and Infrared Imaging Spectrometer Applied in Small Solar System Body Exploration" 5th International Symposium of Space Optical Instruments and Applications, *Springer Proceedings in Physics* 232, 147 (2018)
- [16] Liu, Q., Guo, P., and W.J., "Fabrication of the Partition Multiplexing Convex Grating" *Proc. 5th International Symposium of Space Optical Instruments and Applications, Springer Proceedings in Physics* 232, 197 (2018)
- [17] Borguet, B., Moreau, V., Santandrea, S., Versluys, J., and Bourdoux, A., "The challenges of broadband performances within a compact imaging spectrometer: the ELOIS solution" *Proc. SPIE* 11852, International Conference on Space Optics – ICSO 2020, (2021)
- [18] Stroke, G.W., *Phys. Lett.* 5, 45 (1963)
- [19] Bushkamp, P., Sang, B., Peacocke, P., Pieraccini, S., Geiss, M.J., Roth, C., Moreau, V., Borguet, B., Maresi, L., Rast, M., and Nieke, J., "CHIME's hyperspectral imaging spectrometer design result from phase A/B1" *Proc. SPIE* 11852, International Conference on Space Optics – ICSO 2020, (2021)
- [20] De Clercq, C., Moreau, V., Jamoye, J.F., Zuccaro Marchi, A., and Gloesener, P., « ELOIS: an innovative spectrometer design using a free-form grating », *Proc. SPIE* 9626, 96261O (2015)
- [21] Yew Jin Tan, N., Kumar, A.S., Zhou, G., and Liu, K., "5-Axis ultra-precision shaping of blazed diffraction gratings on high curvature convex ellipsoidal surfaces" *Euspen's 21st international conference and exhibition* (2021)
- [22] Sharpe, M.R., and Irish, D., "A study of light in diffraction grating monochromators", *Optics Acta*, 25, 861-893 (1978)
- [23] Koch, F., Zilk, M., and Glaser, T., "Semi-analytic modeling of diffraction grating BRDF using scalar Fourier optics" *Proc. SPIE* Vol. 11783 (2021)

- [24] Smith, M.A., Berry, S., Parameswaran, L., Holtsberg, C., Siegel, N., Lockwood, R., Chrisp, M.P., Freeman, D., and Rothschild, M. “Design, simulation, and fabrication of three-dimensional microsystem components using grayscale photolithography”, *J. Micro/Nanolithogr. MEMS MOEMS* 18, 043507 (2019)
- [25] Sykora, D.M., and de Groot, P., “Instantaneous measurement Fizeau interferometer with high spatial resolution” *Proc. SPIE 8126, Optical Manufacturing and Testing IX*, 812610 (2011)
- [26] Corzo-Garcia, S.C., Soons, J.A., and Griesmann, U., “Sensing fabrication errors in diffraction gratings using high dynamic range imaging”, *Optics Express*, 27, 15 (2019)